

Phonon-Assisted Crossover from a Nonmagnetic Peierls Insulator to a Magnetic Stoner Metal

Yongcheng Liang,^{1,*} Xun Yuan,^{1,2} Yanfeng Gao,³ Wenqing Zhang,^{2,3,†} and Peihong Zhang^{3,4,‡}

¹College of Engineering Science and Technology, Shanghai Ocean University, Shanghai 201306, China

²State Key Laboratory of High Performance Ceramics and Superfine Microstructures, Shanghai Institute of Ceramics, Chinese Academy of Sciences, Shanghai 200050, China

³Materials Genome Institute and Department of Physics, Shanghai University, Shanghai 200444, China

⁴Department of Physics, University at Buffalo, State University of New York, Buffalo, New York 14260, USA

(Received 16 July 2014; published 21 October 2014)

We report a unique temperature-induced insulator-metal transition in MnB_4 that is accompanied by a simultaneous magnetostructural change from a nonmagnetic monoclinic $mP20$ phase to a magnetic orthorhombic $oP10$ phase. Such a concurring magnetostructural and insulator-metal transformation is a manifestation of a strong competition between Peierls and Stoner mechanisms that governs a crossover from an electron-pairing to an electron-localization scenario in this system. Therefore, the phase stability of MnB_4 is controlled by a subtle interplay among the Peierls mechanism, Stoner mechanism, and phonon free energy. Our findings not only resolve the longstanding magnetostructural puzzle of MnB_4 but also provide a realistic system for the Peierls-Hubbard model.

DOI: 10.1103/PhysRevLett.113.176401

PACS numbers: 71.30.+h, 61.50.Ks, 63.20.-e, 71.20.Be

Transition-metal borides (TMB) continue to be a focus of intense research that has led to the discovery of many novel materials and appealing properties including topological Kondo insulators (e.g., SmB_6) [1–4], ferromagnetic (FM) fluctuations in the antiferromagnetic (AFM) heavy-fermion metals (e.g., CeB_6) [5], the coexistence of metallicity and superhardness (e.g., ReB_2 , CrB_4) [6–9], the coexistence of superconductivity and superhardness (e.g., FeB_4) [10,11], and even the coexistence of superhardness and anomalously low lattice thermal conductivity (e.g., polytypic WB_3 and MoB_3) [12–14]. Among TMB, manganese tetraboride (MnB_4), originally synthesized in 1960 [15], has recently attracted renewed attention not only because of its extreme hardness [16–18], but because it also exhibits intriguing magnetostructural and electronic behavior [19–22]. Based on powder x-ray diffraction data, MnB_4 has long been assigned a monoclinic $mS10$ structure (space group $C2/m$) [23,24]. However, this widely accepted structure [16,17,23–26] has been called into question by recent theoretical and experimental studies [19–22] that have shown that MnB_4 crystallizes in a new monoclinic $mP20$ structure (space group $P2_1/c$). Considering that both CrB_4 [8,9] and FeB_4 [10,11] adopt an orthorhombic $oP10$ structure (space group $Pnmm$) and that Mn lies in between Cr and Fe on the periodic table, it is rather surprising that MnB_4 does not follow the overall trend of the transition metal tetraboride (TMB₄) structural configuration.

On the other hand, the understanding of magnetic and electronic properties of MnB_4 is far from satisfactory. Knappschneider *et al.* [19] synthesized single crystals of MnB_4 under normal-pressure, high-temperature conditions. Their magnetic susceptibility measurements indicate that

MnB_4 is paramagnetic. Further electrical conductivity measurements reveal that it is a semiconductor with a small activation energy of about 0.04 eV. These observations strongly suggest that there might be Peierls-like distortions in MnB_4 , leading to a nonmagnetic (NM) insulating state. Gou *et al.* [20] utilized the high-pressure, high-temperature technique to synthesize single crystals of MnB_4 and also investigated its magnetic behavior. They conclude that MnB_4 exhibits FM spin correlations but shows no long-range magnetic ordering. In addition, they reported that MnB_4 should be metallic since there is a large electronic contribution to the specific heat. These findings are clearly incompatible with the Peierls scenario. To address these open issues, we have carried out an in-depth investigation of the magnetostructural properties of MnB_4 with the hope of reconciling these seemingly inconsistent experimental results.

In this Letter, we present a systematic investigation of the electronic, magnetic, and structural properties of MnB_4 using density functional theory (DFT) based first-principles methods. We find that MnB_4 undergoes a temperature-induced phase transition from the NM insulating state with the $mP20$ structure to a magnetic metallic state with the $oP10$ structure. Equally importantly, we demonstrate that such a simultaneous magnetostructural and insulator-metal transition is a result of a strong competition between Peierls and Stoner mechanisms. To the best of our knowledge, this is the first report that these two mechanisms are both active in one material, resulting in a unique phase transition in MnB_4 .

Our calculations were carried out using spin-polarized DFT as implemented in the VASP code [27]. The all-electron

projector augmented wave method [28] was adopted with $2s^22p^1$ and $3d^64s^1$ treated as valence electrons for B and Mn atoms, respectively. A plane-wave basis set with a large cutoff energy of 500 eV and dense k meshes were employed for the considered phases to ensure that the numerical accuracy can resolve an energy difference of less than 1 meV/atom. Forces on the ions were calculated through the Hellmann-Feynman theorem, allowing a full geometry optimization of the different structures (i.e., $mS10$, $oP10$, and $mP20$) and magnetic phases (i.e., NM, FM, and AFM) of MnB_4 . In order to reveal possible phase transitions, we have investigated free energies of different phases over a wide range of temperature and volume. Phonon calculations were carried out using the PHONOPY package [29] with the force-constant matrices calculated from VASP.

We have carefully checked the sensitivity of the calculated results to different energy functionals, including the generalized gradient approximation (GGA) [30] and local density approximation (LDA) [31], with and without an effective Hubbard U . Our results show that the GGA gives the most faithful overall description of the structural parameters, relative energies, and magnetic and electronic structures of the different phases of MnB_4 , although other methods (e.g., LDA) also reproduce the main results. Therefore, we shall restrict our discussion to the GGA results, unless otherwise specified.

Figure 1(a) shows the calculated total energy as a function of volume for several possible structures and magnetic phases of MnB_4 ; corresponding numerical values of the total energy and local magnetic moment at the respective equilibrium volumes are presented in Table I. We first notice that the $mS10$ structure is the most energetically unfavorable one in all of the different magnetic states (NM, FM, and AFM). In addition, phonon calculations indicate that this structure is dynamically unstable (see Fig. S1 in the Supplemental Material [32]). Hence, we can safely exclude the $mS10$ structure, although it has been a long perceived structure for MnB_4 [23,24]. Unlike the $mS10$ structure for which all three magnetic states can be obtained from our calculations, the spin-polarized calculations for the $mP20$ structure always converge to a NM solution. This NM state has the lowest total energy among all considered phases, suggesting that this is the ground state of MnB_4 . Moreover, phonon calculations show no soft modes for this structure, indicating that this structure is also dynamically stable (see Fig. S2 in the Supplemental Material [32]). Our results therefore support the recent theoretical and experimental proposals of the $mP20$ structure [19–22].

For the $oP10$ structure, the NM state is much higher (by 84.0 meV/f.u.) in energy than the ground state and is dynamically unstable (see Fig. S3 in the Supplemental Material [32]). We thus conclude that MnB_4 cannot assume the NM $oP10$ structure as several other transition metal tetraborides do. However, allowing the development of magnetic moments (about $0.6\mu_B/Mn$) significantly lowers

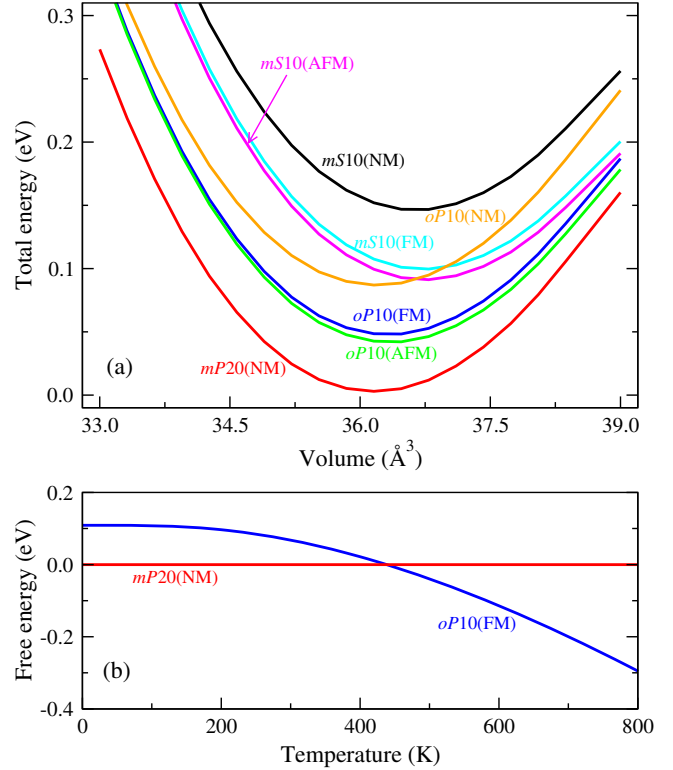


FIG. 1 (color online). (a) Calculated total energy versus volume of different phases of MnB_4 . (b) Relative free energy versus temperature for the $oP10$ (FM) and $mP20$ (NM) phases. The total energy at the equilibrium volume and the free energy of the NM $mP20$ phase are set as the reference energy (i.e., set to zero) in (a) and (b), respectively. All energies are rescaled for one MnB_4 formula unit (f.u.).

the total energy (by about 40 meV/f.u.) of the $oP10$ structure. Remarkably, the formation of local magnetic moments greatly stabilizes the $oP10$ structure and all soft phonon modes disappear (see Fig. S3 in the Supplemental Material [32]). We have calculated both the FM and AFM ordered states and find that they are nearly degenerate (with a difference of about 6 meV/f.u.), indicating a weak magnetic coupling in this system. These results substantiate that the magnetic $oP10$ phase of MnB_4 is a metastable

TABLE I. Calculated relative total energy E (meV/f.u.) and local magnetic moment M (μ_B/Mn) for three possible structures of MnB_4 with different magnetic orderings at respective equilibrium volumes. The energy of the NM $mP20$ phase is set as the reference energy (i.e., set to zero).

		NM	FM	AFM
$mS10$	E	143.5	96.8	88.4
	M	0.0	0.58	0.66
$oP10$	E	84.0	45.0	38.9
	M	0.0	0.59	0.66
$mP20$	E	0.0
	M	0.0

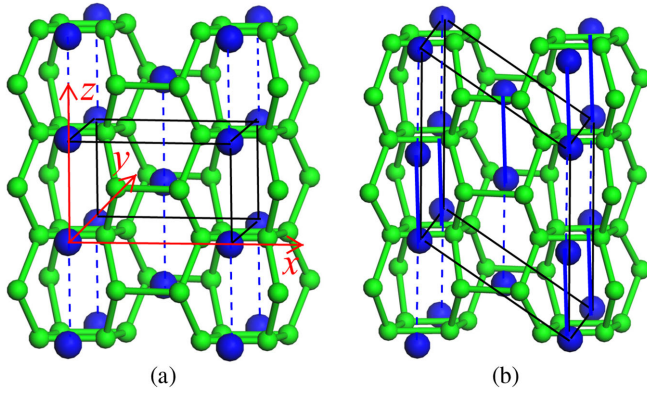


FIG. 2 (color online). Crystal structures of the orthorhombic $oP10$ (a) and monoclinic $mP20$ (b) phases of MnB_4 . The blue (large) and green (small) spheres represent Mn and B atoms, respectively. The low-symmetry $mP20$ structure can be derived from the high-symmetry $oP10$ structure through lattice distortions and dimerization of the Mn atoms. In the $oP10$ structure, the Mn atoms form one-dimensional chains (shown by blue dashed lines) with a uniform Mn-Mn distance. In the $mP20$ structure, the Mn atoms dimerize and form slightly zigzagged chains (shown by alternating blue solid and dashed lines).

phase and should be viable under appropriate conditions. In the following, we only focus on the FM state for simplicity since the AFM state shares many of the general features of the FM state.

As can be seen from Fig. 1(a), there is no crossing between the two energetically competitive phases (NM $mP20$ and FM $oP10$), suggesting that there are no pressure-induced phase transitions at zero temperature. In order to take temperature effects into account, we have calculated the phonon free energy of both phases. As shown in Fig. 1(b), a phase transition from the NM $mP20$ phase to the FM $oP10$ phase takes place at about 440 K. Such a unique magnetostructural phase transformation has never been reported in TMB.

It is puzzling that the magnetostructural behaviors of MnB_4 could be so much different from those of other TMB_4s (e.g., CrB_4 and FeB_4), and several fundamental questions remain to be answered: (1) What is the origin of the instability of the NM $oP10$ phase? (2) What mechanism stabilizes the NM $mP20$ phase? (3) What drives MnB_4 to transform from the NM $mP20$ phase to the FM $oP10$ phase? The answers to these questions must lie in the fundamental structural and electronic properties of the system.

As illustrated in Fig. 2(a), an orthorhombic cell of the $oP10$ structure contains two TMB_4 formulas in which the transition metal (TM) and B atoms locate at the Wyckoff $2a$ and $4g$ sites, respectively. Within planes parallel to (001), the B atoms are linked into groups of four in a parallelogram arrangement and these parallelograms are connected above and below, thus forming a three-dimensional B network (B_4). The interstitial positions of B_4 are occupied by the TM atoms, forming one-dimensional metal chains

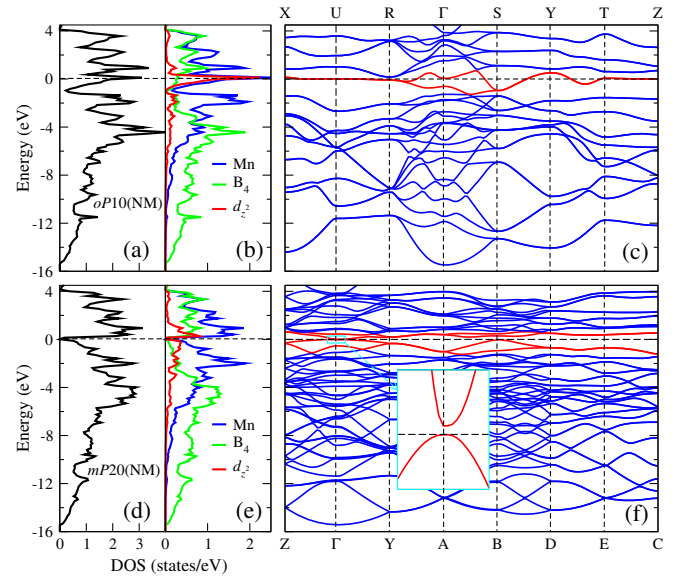


FIG. 3 (color online). Total and projected DOSs and band structures (from left to right) of the NM $oP10$ phase (top panels) and the NM $mP20$ phase (bottom panels) of MnB_4 . The Peierls distortion results in the opening of a small gap at Γ as shown in the inset. The Fermi levels are set at 0 eV and shown as horizontal dashed lines.

in the z direction. Thus, each TM atom is surrounded by twelve B atoms, four in a parallelogram and eight in a parallelepiped, and the TM atoms form one-dimensional chains along the z direction [33,34].

As mentioned above, the NM $oP10$ structure is stable for both CrB_4 and FeB_4 but is unstable for MnB_4 . It is of great interest to understand the electronic origin of this instability. Figures 3(a), 3(b), and 3(c) show the total density of states (DOS), projected DOS, and band structure, respectively, of the NM $oP10$ structure. The lowest six bands in the range of $(-16, -8)$ eV have predominantly B- $2s$ character. The weight of the Mn- $3d$ states increases gradually and there is a strong hybridization between the B- $2p_y(2p_z)$ and Mn- $3d_{xy}(3d_{xz})$ states. The eight bands in the range of $(-8, -3)$ eV may be viewed as the bonding states of the pd hybridization complex, while the six unoccupied bands in the range of $(0.5, 4)$ eV are the corresponding antibonding states. In addition, from -3 to -1 eV, there are four bands which are mainly derived from the Mn- $3d_{x^2-y^2}$ and $3d_{yz}$ states.

The most important feature, a hallmark of instability, is the extremely high DOS at the Fermi level. The fairly flat bands ranging from -1 to 0.5 eV are derived from Mn- $3d_{z^2}$ states as highlighted in red in Figs. 3(b) and 3(c). We can clearly see that the Fermi level lies nearly at the peak position. It is this high DOS at the Fermi level that is responsible for the instability of the NM $oP10$ phase of MnB_4 . In this structure, the Mn atoms form one-dimensional chains in the z direction. Thus the Mn- $3d_{z^2}$ derived states show a strongly one-dimensional character.

Because of the large Mn-Mn distance, the dispersion of the Mn- $3d_{z^2}$ derived bands is very small. Therefore, the instability of the system is attributed to the half-filled, quasi-one-dimensional Mn- $3d_{z^2}$ derived states. In CrB₄ (FeB₄), the Cr- $3d_{z^2}$ (Fe- $3d_{z^2}$) orbitals are fully unoccupied (occupied) and the Fermi level lies at a minimum of the DOS [8,10]; thus, the NM *oP10* structure is stable.

There are two fundamental modes for restoring the stability of a structure with a high DOS at the Fermi level: one is by structural distortion (Peierls mechanism), the other by developing magnetism (Stoner mechanism). The Peierls mechanism breaks the structural degeneracy while the Stoner mechanism lifts the spin degeneracy; both mechanisms may reduce the DOS at the Fermi level and may restore the stability of a material system. However, usually one mechanism dominates, and seldom are both mechanisms active in one material. Exactly which mechanism dominates will then depend on the details of the competition between the electronic (including magnetic) and structural (phonon) degrees of freedom. Interestingly, we find that MnB₄ is such a system where both mechanisms are in action, resulting in rich and complex magnetostructural behaviors of this system.

At low temperatures, the Peierls mechanism is more effective in stabilizing MnB₄, as confirmed by our first-principles calculations [see Fig. 1(b)]. The monoclinic *mP20* structure can be derived from the orthorhombic *oP10* structure by a structural distortion [see Fig. 2(b)]. The basis vectors (*a*, *b*, *c*) of the *mP20* structure correspond to the [0,0,2], [0,1,0], and [-1, 0, -1] lattice vectors of the *oP10* structure, respectively. The angle (90°) between the [1,0,0] and [0,0,1] vectors of the *oP10* structure is changed to 92.117° in the *mP20* structure. As a result of this distortion, the one-dimensional metal chains with a uniform Mn-Mn distance of 2.929 Å are dimerized with alternating distances of 2.702 and 3.198 Å.

The total and projected DOSs of the NM *mP20* phase are presented in Figs. 3(d) and 3(e), respectively. The DOS of the NM *mP20* phase shares many common features with that of the NM *oP10* phase except for the Mn- $3d_{z^2}$ derived states. Because of the dimerization of the Mn atoms, the Mn- $3d_{z^2}$ derived states now split into bonding and antibonding states in the *mP20* structure and a small band gap (about 0.02 eV) develops. Our results not only support the recent experimental observations of the *mP20* phase of MnB₄ with the semiconducting behavior [19], but also explain the origin of the instability of the NM *oP10* phase. We should mention that the band gap could be larger in reality since DFT calculations typically underestimate the band gap of semiconductors and insulators.

Allowing the development of magnetism (the Stoner mechanism) opens up another avenue for the stabilization of MnB₄ through breaking the spin degeneracy. Indeed, we find that the development of local magnetic moments substantially lowers the total energy of the system as

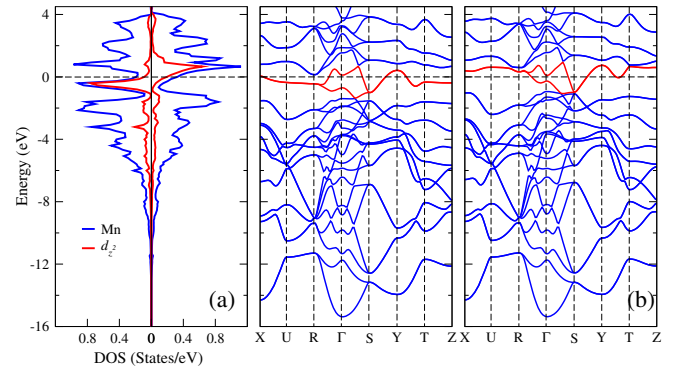


FIG. 4 (color online). Projected DOS (a) and band structures (b) of the FM *oP10* phase of MnB₄. Their left and right panels represent the majority and minority spins, respectively. The Fermi levels are located at 0 eV as indicated by the horizontal dashed lines.

shown in Fig. 1(a) and Table I. The energy of the *oP10* structure is lowered (by about 40 meV/f.u.) compared with the NM phase. Figure 4(a) displays the total and projected DOSs of the FM *oP10* phase; the corresponding band structure is shown in Fig. 4(b). The spin polarization causes a large spin splitting of the Mn- $3d_{z^2}$ states. Despite the strong spin splitting, the system does not develop a full gap and remains metallic. This magnetic *oP10* phase, together with the NM insulating *mP20* phase, successfully explains the seemingly conflicting experimental observations reported earlier [19,20]. Furthermore, the metallic bands exhibit a strong one-dimensional character along the Mn chains. Therefore, the FM *oP10* phase may provide an interesting realistic material system for studying the one-dimensional one-band Peierls-Hubbard model. We would like to mention that in real experiments, the long-range FM ordering is likely destroyed by thermal effects since the magnetic coupling is very weak in this system.

As discussed above, the Peierls mechanism dominates at low temperatures; thus, the system is stabilized into the distorted NM *mP20* structure. However, as the temperature rises, the vibrational entropy becomes an important driving force for the structural phase transition in MnB₄. Taking into account the contribution from phonons, the free energy of the FM *oP10* phase decreases relative to that of the NM *mP20* phase with increasing temperature, eventually falling below that of the NM *mP20* phase above 440 K as shown in Fig. 1(b). We would like to emphasize that this phase transition is different from a purely Stoner mechanism: it is a temperature (phonon) assisted phase transition from a NM Peierls insulator at low temperatures to a FM Stoner metal at high temperatures.

In summary, we have identified a temperature-induced insulator-metal transition in MnB₄ that is accompanied by a simultaneously magnetostructural change from the NM monoclinic *mP20* phase to the magnetic orthorhombic *oP10* phase. At low temperatures, the low-symmetry *mP20*

structure is stabilized by a Peierls distortion, leading to the NM insulating state. As the temperature increases, the high-symmetry $oP10$ structure is preferred. The high DOS at the Fermi level, however, strongly drives it towards the Stoner instability, resulting in the magnetic metal at high temperatures. Such a simultaneous magnetostructural and insular-metal phase transition arises from the unique competition among the Peierls mechanism, Stoner mechanism, and phonon free-energy that has never been observed in other TMB. The present work not only resolves the puzzling magnetostructural issue of this class of TMB₄s but also provides a realistic material system for the Peierls-Hubbard model [35,36].

This work is supported by the National Natural Science Foundation of China (Grants No. 51072213, No. 11328401, and No. 11234012), the State Oceanic Administration (Grant No. SHME2013JS01), and the Science and Technology Commission of Shanghai Municipality (Grants No. 13JC1402900, No. 11JC1404700, and No. 14XD1424300). Work at U.B. is supported by the U.S. Department of Energy under Grant No. DE-SC0002623.

*ycliang@shou.edu.cn

†wqzhang@mail.sic.ac.cn

‡pzhang3@buffalo.edu

- [1] M. Neupane, N. Alidoust, S.-Y. Xu, T. Kondo, Y. Ishida, D. J. Kim, Chang Liu, I. Belopolski, Y. J. Jo, T.-R. Chang, H.-T. Jeng, T. Durakiewicz, L. Balicas, H. Lin, A. Bansil, S. Shin, Z. Fisk, and M. Z. Hasan, *Nat. Commun.* **4**, 2991 (2013).
- [2] D. J. Kim, J. Xia, and Z. Fisk, *Nat. Mater.* **13**, 466 (2014).
- [3] H. Weng, J. Zhao, Z. Wang, Z. Fang, and X. Dai, *Phys. Rev. Lett.* **112**, 016403 (2014).
- [4] C.-H. Min, P. Lutz, S. Fiedler, B. Y. Kang, B. K. Cho, H.-D. Kim, H. Bentmann, and F. Reinert, *Phys. Rev. Lett.* **112**, 226402 (2014).
- [5] H. Jang, G. Friemel, J. Ollivier, A. V. Dukhnenko, N. Yu. Shitsevalova, V. B. Filipov, B. Keimer, and D. S. Inosov, *Nat. Mater.* **13**, 682 (2014).
- [6] H. Y. Chung, M. B. Weinberger, J. B. Levine, A. Kavner, J. M. Yang, S. H. Tolbert, and R. B. Kaner, *Science* **316**, 436 (2007).
- [7] Y. Liang and B. Zhang, *Phys. Rev. B* **76**, 132101 (2007).
- [8] H. Niu, J. Wang, X. Q. Chen, D. Li, Y. Li, P. Lazar, R. Podloucky, and A. N. Kolmogorov, *Phys. Rev. B* **85**, 144116 (2012).
- [9] A. Knappschneider, C. Litterscheid, D. Dzivenko, J. A. Kurzman, R. Seshadri, N. Wagner, J. Beck, R. Riedel, and B. Albert, *Inorg. Chem.* **52**, 540 (2013).
- [10] A. N. Kolmogorov, S. Shah, E. R. Margine, A. F. Bialon, T. Hammerschmidt, and R. Drautz, *Phys. Rev. Lett.* **105**, 217003 (2010).
- [11] H. Gou, N. Dubrovinskaia, E. Bykova, A. A. Tsirlin, D. Kasinathan, W. Schnelle, A. Richter, M. Merlini, M. Hanfland, A. M. Abakumov, D. Batuk, G. Van Tendeloo, Y. Nakajima, A. N. Kolmogorov, and L. Dubrovinsky, *Phys. Rev. Lett.* **111**, 157002 (2013).
- [12] Y. Liang, X. Yuan, and W. Zhang, *Phys. Rev. B* **83**, 220102 (R) (2011).
- [13] Y. Liang, X. Yuan, Z. Fu, Y. Li, and Z. Zhong, *Appl. Phys. Lett.* **101**, 181908 (2012).
- [14] Y. Liang, J. Yang, X. Yuan, W. Qiu, Z. Zhong, J. Yang, and W. Zhang, *Sci. Rep.* **4**, 05063 (2014).
- [15] R. Fruchart and A. Michel, *Compt. Rend.* **251**, 2953 (1960).
- [16] B. Wang, X. Li, Y. X. Wang, and Y. F. Tu, *J. Phys. Chem. C* **115**, 21429 (2011).
- [17] H. Gou, Z. Li, H. Niu, F. Gao, J. Zhang, R. C. Ewing, and J. Lian, *Appl. Phys. Lett.* **100**, 111907 (2012).
- [18] M. Yang, Y. Wang, J. Yao, Z. Li, J. Zhang, L. Wu, H. Li, J. Zhang, and H. Gou, *J. Solid State Chem.* **213**, 52 (2014).
- [19] A. Knappschneider, C. Litterscheid, N. C. George, J. Brgoch, N. Wagner, J. Beck, J. A. Kurzman, R. Seshadri, and B. Albert, *Angew. Chem., Int. Ed. Engl.* **53**, 1684 (2014).
- [20] H. Gou, A. A. Tsirlin, E. Bykova, A. M. Abakumov, G. Van Tendeloo, A. Richter, S. V. Ovsyannikov, A. V. Kurnosov, D. M. Trots, Z. Konopkova, H. P. Liermann, L. Dubrovinsky, and N. Dubrovinskaia, *Phys. Rev. B* **89**, 064108 (2014).
- [21] H. Niu, X.-Q. Chen, W. Ren, Q. Zhu, A. R. Oganov, D. Li, and Y. Li, *Phys. Chem. Chem. Phys.* **16**, 15866 (2014).
- [22] A. G. Van Der Geest and A. N. Kolmogorov, *CALPHAD* **46**, 184 (2014).
- [23] S. Andersson, *Acta Chem. Scand.* **23**, 687 (1969).
- [24] S. Andersson and J.-O. Carlsson, *Acta Chem. Scand.* **24**, 1791 (1970).
- [25] J. K. Burdett and E. Canadell, *Inorg. Chem.* **27**, 4437 (1988).
- [26] X. Meng, K. Bao, P. Zhu, Z. He, Q. Tao, J. Li, Z. Mao, and T. Cui, *J. Appl. Phys.* **111**, 112616 (2012).
- [27] G. Kresse and J. Furthmuller, *Phys. Rev. B* **54**, 11169 (1996).
- [28] P. E. Blochl, *Phys. Rev. B* **50**, 17953 (1994).
- [29] A. Togo, F. Oba, and I. Tanaka, *Phys. Rev. B* **78**, 134106 (2008).
- [30] J. P. Perdew, K. Burke, and M. Ernzerhof, *Phys. Rev. Lett.* **77**, 3865 (1996).
- [31] J. P. Perdew and Y. Wang, *Phys. Rev. B* **45**, 13244 (1992).
- [32] See the Supplemental Material at <http://link.aps.org/supplemental/10.1103/PhysRevLett.113.176401> for details of the dynamical stability of different structural and magnetic phases of MnB₄.
- [33] Y. Liang, Z. Zhong, and W. Zhang, *Comput. Mater. Sci.* **68**, 222 (2013).
- [34] Y. Gou, Z. Fu, Y. Liang, Z. Zhong, and S. Wang, *Solid State Commun.* **187**, 28 (2014).
- [35] I. Egri, *Solid State Commun.* **17**, 441 (1975).
- [36] S. Mazumdar and S. N. Dixit, *Phys. Rev. Lett.* **51**, 292 (1983).